Gypsum scaling in forward osmosis: Role of membrane surface chemistry

Gypsum Scaling in Forward Osmosis: Role of Membrane Surface Chemistry

Journal of Membrane Sciences

Revised: 6 April, 2016

Ming Xie [1*] and Stephen R. Gray [1]

[1] Institute for Sustainability and Innovation, College of Engineering and Science, Victoria University, PO Box 14428, Melbourne, Victoria 8001, Australia

* Corresponding author; Email: ming.xie@vu.edu.au ; Ph: +61 3 9919 8174

ABSTRACT

Forward osmosis (FO) membranes with varying surface chemical functionalities respond differently to gypsum scaling. Using a real-time monitoring system, gypsum scaling was quantified between an asymmetric cellulose triacetate (CTA) and a thin-film composite (TFC) polyamide membrane in terms of water flux decline, gypsum surface coverage and gypsum crystal morphology. At the same initial water flux, the TFC membrane was subjected to more severe gypsum scaling than the CTA membrane in terms of water flux decline and gypsum crystal surface coverage. The gypsum crystal morphology on the CTA membrane featured with slender platelets; in contrast, that on the TFC membrane demonstrated the formation of rosette arrangements. Fourier transform infrared spectra and X-ray photoelectron spectroscopy proved that the gypsum scaling on CTA membrane was dominated by bulk crystallisation with subsequent deposition; while that on the TFC membrane was driven by surface crystallisation via specific interaction between carboxylic functional groups and calcium ions. No interaction between gypsum and CTA membrane surface was demonstrated by the largely unchanged ratio of wavenumbers 1740 cm^{-1} (C=O stretching) to 1366 cm^{-1} (C-O stretching), as well as binding energy of C1s on the CTA membrane. In contrast, specific interaction between carboxylic functional groups with calcium ions during gypsum scaling was revealed by a gradual increase in the ratio of absorbance wavenumber 3400 cm^{-1} (O-H stretching) to 2970 cm^{-1} (C-H stretching), and the occurrence of the carboxylate functional group at binding energy of 288.1 eV on the TFC membrane during the formation of gypsum scaling.

Keywords: forward osmosis; gypsum scaling; cellulose triacetate; polyamide; Fourier transform infrared spectroscopy; X-ray photoelectron spectroscopy

1. Introduction

Forward osmosis (FO), an osmosis-driven membrane process, could potentially advance desalination and wastewater reuse. FO utilises the osmotic pressure of a highly concentrated draw solution as the driving force to transfer water from the feed solution to the draw solution through a dense polymeric membrane. FO has demonstrated a much lower fouling propensity and higher fouling reversibility than RO, which was attributed to the lack of applied hydraulic pressure [1-4]. Consequently, FO is widely used to treat low quality feedwaters, including landfill leachate [5], anaerobic digester concentrate [6], activated sludge solution [7, 8], and municipal wastewater [9-11].

The core of FO membrane has advanced from asymmetric cellulose triacetate (CTA) membrane to polyamide thin-film composite (TFC) membranes because of the excellent mass transfer properties of polyamide [12-14]. Indeed, the TFC membrane not only produces higher water permeability but also exhibits better contaminant rejections in comparison with the CTA membrane. For example, the TFC membrane achieved rejections of four pharmaceuticals above 95%; in contrast, the CTA membrane exhibited varying rejections of these compounds from 65% to 95% [15]. This better performance of the TFC membrane was further demonstrated by substantially higher rejections of neutral contaminants than the CTA membrane [16].

Membrane surface chemistry of CTA and TFC membranes are markedly different. Unlike the CTA membrane abundant with hydroxyl functional groups, the TFC membrane is characterized by a high density of carboxylic acid functional groups, which results in potentially high fouling propensity. Previous knowledge from RO membrane fouling demonstrated that carboxylic functional groups enabled the formation of calcium bridging between the membrane surface and a wide range of organic foulants, and consequently increased organic fouling. Wu et al. [17] found that the carboxylic functional groups on RO membrane exhibited the highest initial alginate adsorption rate in seawater desalination. This higher adsorption was further revealed by measuring the alginate – membrane surface intermolecular force [18], which increased with higher density of carboxylic functional groups.

Role of membrane surface chemistry in FO membrane fouling is conflicting and not well understood. Limited investigations were conducted to compare FO membrane fouling behaviour

between CTA and TFC membranes with different surface chemical functionalities. For instance, more severe gypsum scaling of the TFC membrane was observed in comparison with the CTA membrane [19, 20], which was attributed to stronger adhesion force measured by atomic force measurement (AFM). In contrast, negligible difference in water flux decline was observed between the TFC and CTA membranes during silica scaling. In addition, the adhesion force measurement by AFM also showed stronger hydrogen bonding between silica and the CTA membrane abundant with hydroxyl functional groups [20]. As a result, the role of membrane surface chemistry on FO fouling is not straightforward and necessitates systematic investigation.

In this study, we investigated the role of FO membrane surface chemistry on gypsum scaling using CTA and TFC membranes. Membrane surface chemistry – surface charge and surface functional groups – were characterized. Gypsum scaling of the CTA and TFC membranes was conducted in a real-time observation setup and was quantified in terms of water flux decline, gypsum surface coverage and gypsum crystal morphology. Fourier transform infrared spectroscopy and X-ray photoelectron spectroscopy were used to capture changes of membrane surface chemistry on the CTA and TFC membranes during gypsum scaling, thereby elucidating the role of membrane surface chemistry on gypsum scaling in FO process. We provided, for the first time, a time-resolved gypsum scaling profile of CTA and TFC membranes in FO process. The real-time observation, microscopic imaging as well as comprehensive membrane surface chemistry characterization constituted compelling experimental evidence to elucidate the scaling mechanism from the membrane surface chemistry perspective.

2. Materials and methods

2.1. FO membranes

An asymmetric cellulose triacetate (CTA) and a polyamide thin-film composite (TFC) forward osmosis (FO) membrane were employed in this study. The CTA membrane was composed of a cellulose triacetate layer with an embedded woven support mesh [21, 22]. The TFC membrane was made of a thin selective polyamide active layer on top of a porous polysulfone support layer [23, 24].

2.2. Real-time observation FO setup

A transparent acrylic FO membrane cell coupled with microscopic observation enabled real-time observation of gypsum scaling on membrane surface (Figure S1, Supplementary Data). Specifically, a membrane coupon with an effective area of 20.2 cm^2 was placed in a transparent FO membrane cell. Crossflow rate of 1 L/min (corresponding to crossflow velocity of 9 cm/s) was maintained for both the feed and draw solutions using micro gear pumps. The FO water flux was determined by measuring the weight changes of the feed solution at specific time intervals with a precision balance connected to a computer and a data logging system.

Real-time membrane surface images of 2048 × 1536 pixels resolution were recorded using a high resolution digital camera and an optical microscope (20× magnification). To minimize the interference from air bubbles, the feed and draw solutions were degassed prior to circulation in the FO setup. Through the combination of optical magnification along with a unique combination of bright and low angle dark field illumination, provided by ultra-bright fibre optic illuminator, digital image capture and analysis processing, occurrence and subtle changes of gypsum crystal could be effectively monitored. Recorded images of the scaled membrane surface were processed with image analysis softwares – Image J and Adobe Photoshop – to quantify the time evolution of gypsum surface coverage.

2.3. Experimental procedure of membrane scaling

Both CTA and TFC FO membranes were employed in the gypsum scaling experiments. Varying initial water fluxes of the CTA and TFC membranes were achieved by using different

concentrations of NaCl. The evolution of gypsum scaling of the CTA and TFC membranes were continuously monitored by the real-time observation FO setup.

The protocol for all gypsum scaling experiments comprised the following steps. First, a new membrane coupon, with the active layer facing the feed solution, was placed in the membrane cell before each experiment and stabilised to obtain a constant flux. The stabilization process took about one hour for FO. The membrane in the FO mode was stabilised with deionised water as the feed and varying concentration of NaCl as the draw solution to induce different initial water flux. Next, the gypsum scaling experiment was performed for about 24 h to obtain approximately 1400 mL cumulative permeate volume at the conclusion of each experiment. The gypsum scaling solution was comprised of 35 mM $CaCl_2$, 20mM Na_2SO_4, and 19 mM NaCl, with a gypsum ($CaSO_4 \cdot 2H_2O$) saturation index (SI) of 1.3. Other experimental conditions were: cross-flow rate of 1 L/min (corresponding to the cross-flow velocity of 8.5 cm/s), ambient pH (pH 6.8), and temperature of 25.0 ± 0.1°C. Scaling experiment was operated for around 25 hours, attaining cumulative permeate volume of 1.4 L. Water flux was continuously monitored throughout the fouling experiments by a data logger. A baseline experiment (i.e., feed without $CaCl_2$ and Na_2SO_4) was also carried out to correct the flux decline due to the continuous concentration of the feed solution and dilution of the draw solution, as described in our previous publication [25]. The real-time monitoring system captured images of the FO membrane surface every hour to identify the occurrence of and development of gypsum crystals on FO membrane surface during scaling experiment.

2.4. Relating gypsum scaling to membrane surface chemistry

A suite of techniques were employed to elucidate the mechanisms of gypsum scaling on CTA and TFC membranes whose membrane surface chemistry was markedly different. Specifically, for pristine membranes, surface charge and major functional groups of CTA and TFC membranes were characterised by streaming potential and x-ray photoelectron spectroscopy (XPS). For gypsum-scaled membranes, the morphology of gypsum scaling layer on CTA and TFC membranes was examined by scanning electron microscopy (SEM); changes in bonding chemistry of the CTA and TFC membranes after gypsum scaling was quantified by a high

resolution C1s scan using XPS. In addition, the evolution of gypsum scaling on CTA and TFC membrane surface was observed by Fourier transform infrared spectroscopy (FTIR).

2.4.1 Streaming potential measurement

Membrane surface charge was determined using a SurPASS electrokinetic analyser (Anton Paar GmbH, Graz, Austria). The zeta potential of each membrane surface was calculated from the measured streaming potential using the Fairbrother-Mastin approach [26]. All streaming potential measurements were conducted in a background electrolyte solution containing 10 mM KCl. Hydrochloric acid and potassium hydroxide were used to adjust pH by means of automatic titration. The test solution was used to flush the cell thoroughly prior to pH adjustment for each measurement. All streaming potential measurements were performed at room temperature (22.0 ± 0.1 ºC), which was monitored by the temperature probe of the instrument.

2.4.2 Scanning electron microscopy

The morphology of the gypsum scaling layer on CTA and TFC membrane was characterised using a scanning electron microscopy (SEM) (JEOL JCM-6000, Tokyo, Japan). Prior to SEM analysis, scaled membrane samples were air-dried in a desiccator and were subsequently sputter coated with an ultra-thin layer of gold.

2.4.3 Fourier transform infrared spectroscopy

Gypsum scaling evolution in the initial stage (eight hours) on CTA and TFC membranes were also assessed by Fourier transform infrared spectroscopy with attenuated total reflectance (FTIR-ATR). For each specific time interval, a new membrane coupon was used for gypsum scaling experiment. The gypsum-scaled membrane coupon was air dried for at least 24 h before spectra were measured on an FTIR spectrometer (Thermo Scientific Nicolet 6700) equipped with an ATR accessory consisting of a ZnSe plate (45° angle of incidence). Absorbance spectra were measured with 64 scans of each sample at a spectral resolution of 2 cm^{-1}. Background measurements in air were collected before each membrane sample measurement. ATR-FTIR spectra were collected at two different spots for each membrane sample. The characteristic wavenumbers for the CTA and TFC membranes were summarised in Table S1, Supplementary Data.

2.4.4 X-ray photoelectron spectroscopy

Bond chemistry of membrane surface layer was analysed by high resolution C1s scan with XPS. Specifically, XPS analysis used monochromatic aluminium Kα X-ray photoelectron spectrometer (Thermo Scientific, MA). A spot size of 400 µm was used to scan in the region of the C1s binding energy at 20 eV pass energy. Two random spots on duplicate membrane samples were selected. Excessive charging of the samples was minimized using an electron flood gun. High resolution scans had a resolution of 0.1 eV. Calibration for the elemental binding energy was done based on the reference for C1s at 284.6 eV. Data were processed by standard software with Shirley background and relative sensitivity factor of 0.278 for C1s peaks. The high resolution XPS spectra were subtracted by the Shirley-type background, and Gaussian-Lorentz peak deconvolution was performed to estimate the binding energy shift of carbon C1s. For each membrane type, the deconvoluted peaks were normalized against the peak at the lowest binding energy (corrected to 284.6 eV). The characteristic C1s binding energies for the CTA and TFC membranes were tabulated in Table S2, Supplementary Data. The signal residual after deconvolution was also plotted to assure the accuracy (Figure S4, Supplementary Data).

3. Results and Discussion

3.1. Membrane surface chemistry properties

CTA and TFC membranes possess markedly different surface chemistry properties (Figure 1). The nature of the functional groups of CTA membrane was identified by the shifts in the binding energy of the deconvoluted XPS peak spectra [27, 28] as -C-H- (284.6 eV) and -C-OH (286.2 eV) (Figure 1A); while in contrast, that of the TFC membrane was revealed as -C-H- (284.6 eV), -C=O (286.7 eV), and –COOH (288.9 eV) (Figure 1B) [29-31]. Indeed, the elemental survey by XPS analysis also showed the presence of nitrogen on TFC membrane surface, but was not detected on CTA membrane surface (Figure S2, Supplementary Data). The results demonstrated that the CTA membrane was abundant with hydroxyl functional group, while the TFC membrane was rich in carboxylic functional group.

The significant variation in surface functional groups also resulted in different membrane surface charge. Zeta potential measurements suggested that the surface of the TFC membrane was significantly more negatively charged than that of the CTA membrane at an experimental pH of 6.8 (Figure 1C). The highly negatively charged surface of the TFC membrane can be attributed to the dissociation of free or uncross-linked carboxylic functional groups of the polyamide active skin layer (Petersen 1993). By contrast, the predominant functional group on the CTA membrane surface is hydroxyl, which can only be deprotonated at high pH. Indeed, previous measurement using a toluidine blue O method showed that the number of negatively charged functional groups was negligible on CTA membrane surface [32]. The marginal negative charge of the CTA membrane can be attributed to preferential adsorption of anions, such as chloride and hydroxide, onto the membrane surface [33, 34].

FTIR spectra of pristine CTA and TFC membranes also confirmed the presence of hydroxyl and carboxylic functional groups, respectively (Figure 1D). The CTA membrane was identified by wavenumber of 1740 cm^{-1} (ester C=O stretching in cellulose triacetate) and 1366 cm^{-1} (C-O stretching in hydroxyl functional group) [29, 35]. The TFC membrane exhibited its distinctive amide bands at wave numbers of 1778 and 1719 cm^{-1} (symmetric and asymmetric C=O stretching, respectively), 1378 cm^{-1} (C-N-C stretching), and 1110 cm^{-1} (amide ring) [30, 36]. In addition, in the high wavenumbers, the TFC membrane also showed a broad peak at wavenumber of 3400 cm^{-1} (O-H stretching) and a sharp peak at 2970 cm^{-1} (C-H stretching) [31, 35], respectively, which indicated the presence of carboxylic functional groups on the membrane surface. It is hypothesized that the CTA and TFC membranes abundant with hydroxyl and carboxylic functional groups, respectively, could respond differently to gypsum scaling.

[Figure 1]

3.2. Membrane scaling behaviours

3.2.1. Role of initial water flux

Different initial water flux resulted in notably different water flux decline for both CTA and TFC membranes during gypsum scaling (Figure 2). At low initial water flux of 5 $L.m^{-2}.h^{-1}$, both CTA and TFC membranes exhibited negligible water flux decline. In contrast, with the increase of the initial water flux from 10 to 25 $Lm^{-2}h^{-1}$, the water flux decline of both membranes

was aggravated, with more than 50% water flux decline at the conclusion of the experiment for initial water fluxes of 25 $Lm^{-2}h^{-1}$ (Figure 2). Such initial water flux dependent gypsum scaling behaviour agreed with previous FO fouling observations using varying model foulants, such as, latex particles [37], humic acid [38] and microalgae [39]. These previous studies also reported more severe water flux decline when the FO membrane was operated at higher initial water flux.

[Figure 2]

The initial water flux dependent gypsum scaling behaviour was also revealed by real-time observation technique. A strong correlation between percentage of water flux decline and membrane surface coverage by gypsum was observed (Figure 3). Specifically, for the CTA membrane, when initial water flux increased from 5 to 25 $Lm^{-2}h^{-1}$, the percentage of water flux decline increased from 5% to 45% at the conclusion of the experiment, which was driven by an increase in membrane surface coverage from 17% to 42% (Figure 3A). Similarly, TFC membrane also demonstrated similar increase in the percentage of water flux decline as well membrane surface coverage when the initial water flux increased from 5 to 25 $Lm^{-2}h^{-1}$ (Figure 3B).

Notably, TFC membrane was subject to more severe gypsum scaling in comparison with CTA membrane (Figure 3). For instance, under the same initial water flux of 25 $Lm^{-2}h^{-1}$, water flux decline as well as membrane surface coverage by the TFC membrane (65% water flux decline and 67% membrane surface coverage) was significantly higher than those by the CTA membrane (45% water flux decline and 43% membrane surface coverage).

Such variation in the CTA and TFC membrane gypsum scaling warrants an in-depth examination of gypsum scaling evolution to elucidate the underlying mechanism. Previous study compared gypsum scaling on polyamide and cellulose membrane by measuring the adhesion force using model gypsum crystal [19], hypothesizing that the gypsum scaling on polyamide membrane was dominated by surface crystallisation, while that on cellulose membrane was controlled by bulk crystallisation. A detailed membrane surface chemistry analysis as well as an *in situ* experimental approach can further advance and shed light on our understanding of gypsum scaling on different membrane surface chemistries.

[Figure 3]

3.2.2. Scaling evolution

Gypsum scaling evolution of the CTA and TFC membranes were quantified by the real-time observation technique. Development of gypsum scaling layer on the CTA and TFC membranes were imaged at specific cumulative permeate volume (Figure 4). Visually, gypsum scaling on the TFC membrane was not only more severe, but also progressed more rapidly in comparison with the CTA membrane. Indeed, early gypsum scaling on TFC membrane was visualised even at cumulative permeate volume of 400 mL (corresponding to 6 hours of filtration). At the conclusion of gypsum scaling experiments, the coverage of gypsum scaling layer on the TFC membrane was more extensive than that on the CTA membrane.

[Figure 4]

This real-time visualisation was consistent with a detailed membrane surface coverage analysis for the CTA and TFC membranes (Figure 5A). Specifically, the quantified membrane surface coverage demonstrated that the evolution of gypsum scaling of the TFC membrane was more rapid and severe than the CTA membrane. More importantly, the morphology of gypsum scaling was markedly different between CTA and TFC membranes (Figure 5B and C), suggesting different scaling mechanisms on these two membranes. Indeed, the crystal-covered CTA membrane images in Figure 5C suggest that gypsum crystals found on the surface consist of slender platelets and rods in the size range of 20-100 μm and remnants of rosettes, which are believed to have been fractured by bulk crystal deposition. Indeed, the gypsum crystal size range on the CTA membrane surface was consistent with the size distribution measured by Zetasizer Nano ZSP (Malvern, Worcestershire, UK) (Figure S3, Supplementary Data). In contrast, gypsum scaling on the TFC membrane demonstrated the formation of rosette arrangements consisting of gypsum needles originating from a core growth region on the membrane surface with size of 300 μm (Figure 5B), which suggested the domination of surface crystallization.

[Figure 5]

The real-time experimental approach together with a wide range of initial water fluxes employed here provided a distinctively different the gypsum scaling behaviour on CTA and TFC membrane. In addition, the experimental evidence opens an opportunity to track the gypsum

scaling on both CTA and TFC membrane in a time-resolved manner, which was a significant advancement in comparison with previous literature [19].

3.3. Membrane surface chemistry plays an important role in gypsum scaling

Markedly different gypsum scaling behaviour, together with contrasted gypsum crystal morphology on the CTA and TFC membranes suggested different gypsum scaling mechanisms. Therefore, it is hypothesized that the CTA and TFC membranes, which possesses different membrane surface chemistry, respond differently to the gypsum scaling. Specifically, the CTA membrane, abundant with hydroxyl functional groups, was dominated by gypsum bulk crystallisation and subsequent particle deposition; by contrast, the TFC membrane, rich in carboxylic functional groups, is largely influenced by gypsum surface crystallisation via specific interaction between membrane carboxylic functional groups and calcium ions.

Further evidence is provided to support this hypothesis by tracking changes in CTA and TFC membrane surface chemistry by ATR-FTIR, as well as C1s binding energy shift of CTA and TFC membrane surface by XPS.

3.3.1. FTIR

Changes in CTA and TFC membrane surface functional groups at the initial stage of gypsum scaling were monitored by ATR-FTIR (Figure 6). The reference wavenumbers were selected to demonstrate the interaction between gypsum and membrane interface, which can be sensitively detected by the ATR-FTIR technique. The wavenumber that represents membrane functional groups associated with the gypsum scaling were identified. The C=O stretching was one characteristic wavenumber in the cellulose triacetate membrane where the C=O bond was available in the structure of triacetate due to the phase inversion synthesis procedure. In addition, ATR-FTIR is more surface sensitive in the high wave number region with a penetration depth less than ~200 nm over 4000-2600 cm^{-1}. The penetration depth is greater than 300 nm at wavenumbers lower than 2000 cm^{-1}, which means the chemical information of both the active layer and polysulfone support layer can be obtained in the TFC membrane at wavenumbers below 2000 cm^{-1}. The low wavenumber signal cannot be attributed to the interfacial interaction between gypsum and TFC active layer alone. As a result, high wavenumbers (2970 cm^{-1} and 3400 cm^{-1}) were used to track the gypsum scaling at the TFC membrane interface.

The ATR-FTIR spectra were used as a qualitative indicator of gypsum scaling on membrane surface. The response of CTA membrane to gypsum scaling was revealed by the ratio of absorbance at wavenumbers indicative of major functional groups on the CTA membrane surface, specifically 1740 cm^{-1} and 1366 cm^{-1}, representing the C=O stretching and C-O stretching in the ester and hydroxyl functional groups. The largely unchanged ratio of these two wave numbers (I_{1740}/I_{1366}) showed that there was no interaction between gypsum and CTA membrane surface. Reduction of absorbance at these two wave numbers was mainly driven by the deposition of gypsum on the CTA membrane surface, thereby reducing the penetration depth of IR beam and the collected absorbance signal.

[Figure 6]

For the TFC membrane, progressive gypsum scaling was evident by two characteristic wave numbers of 3400 cm^{-1} and 2970 cm^{-1}, which represented O-H stretching and C-H stretching on the TFC membrane surface, respectively [40]. A gradual increase in the ratio of absorbance at wavenumbers of 3400 cm^{-1} to 2970 cm^{-1} (I_{3400}/I_{2970}) was observed as gypsum scaling progressed. This increase was mainly driven by the increased absorbance at 3400 cm^{-1}. The notable increase suggested the occurrence of specific interaction between carboxylic functional groups with calcium ions during gypsum scaling. The calcium ions formed complexes with carboxylic functional groups on TFC membrane surface. As a result, the formation of calcium carboxylate on the TFC membrane induced stronger stretching of the O-H, which also enhanced calcium concentration on the membrane surface, thereby initiating the formation of gypsum pre-nucleation crystals, and subsequently gypsum surface crystallisation.

3.3.2. Binding energy shift of *C1s*

To further elucidate the interaction between gypsum and membrane surface during gypsum scaling, high resolution XPS scans were performed to examine the binding energy shift of C1s of the CTA and TFC membranes after gypsum scaling. Specifically, no new peak was identified on the CTA membrane after gypsum scaling (Figure 7A and Figure 1A), where the major bonds were C-H and C-OH. This observation was consistent with the largely unchanged absorbance ratio of the FTIR spectra during gypsum scaling (Figure 6A). As a result, the CTA membrane with the predominant hydroxyl functional groups is neutral and does not have specific

interactions with calcium. Thus, it has much lower probability for gypsum to form pre-nucleation crystals and precipitate directly on CTA membrane surfaces. The observations from FTIR spectra and XPS scan supported the hypothesis that the gypsum scaling on the CTA membrane was governed by crystallisation taking place in the bulk solution, which has negligible interaction with the membrane functional groups.

[Figure 7]

By contrast, in addition to the carboxylic functional group at binding energy of 289.5 eV, carboxylate functional groups were observed at binding energy of 288.1 eV on the TFC membrane after gypsum scaling. The binding energy of 288.1 eV has been characterised as carboxylic functional group, which can be in the form of carboxylic acid or the coordination with calcium carboxylate [41, 42]. This result also agreed with the FTIR spectra collected during the gypsum scaling (Figure 6B). The electrostatic attraction between negatively charged carboxylic functional groups and positively charged calcium ions stretched the C-OH functional groups, and formed calcium carboxylate electrovalent coordination bonds. As a result, this observation by XPS and FTIR spectra confirmed the hypothesis that calcium ions have specific interaction with carboxylic functional group on the TFC membrane, and thus facilitates the formation of prenucleation crystals on the membrane surface, thereby inducing surface crystallisation.

Results showed here also agreed with previous studies comparing gypsum scaling on CTA and TFC membranes. Mi and Elimelech [19] observed that the adhesion force between gypsum particle and TFC membrane was significantly higher than that with CTA membrane. However, via FTIR and XPS techniques, our work utilised a real-time approach to provide an in-situ understanding in the gypsum-membrane interaction. Particularly, tracking intensity change in specific wavenumbers by FTIR enabled a swift response of gypsum-membrane interaction from the perspective of characteristic functional groups. Further to this FTIR technique, our high resolution XPS spectra clearly showed the presence of calcium carboxylic groups in gypsum scaling on TFC membrane. Both experimental results provide a clear picture of how gypsum interacted with the carboxylic functional groups on TFC membrane. The perspective from membrane surface chemistry is one step forward in comparison to the indirect force measurement used in comparison with previous work [19].

As a result, it was suggested that gypsum scaling of TFC membrane was dominated by heterogeneous crystallization, while that of the CTA membrane was dominated by bulk crystallization. More importantly, these studies proposed that the adhesion force between foulant and TFC membrane surface was greater than the CTA membrane, thereby significantly decreasing the cleaning efficiency of the TFC membrane. The experimental observation also has significant implication in providing a foundation for effective FO gypsum scaling mitigation by controlling the membrane surface chemistry, which is critical to the next generation FO membrane development in treatment of challenging waste streams.

4. Conclusion

Results reported here demonstrated that membrane surface chemistry played an important role in gypsum scaling in FO process. Gypsum scaling, characterised by water flux decline and gypsum crystal surface coverage using real-time observation technique, became more severe for both CTA and TFC membranes as the initial water flux increases. However, at the same initial water flux, the TFC membrane was subjected to more severe gypsum scaling than the CTA membrane in terms of water flux and gypsum crystal surface coverage. More importantly, the gypsum crystal morphology on the CTA featured slender platelets; by contrast, that on the TFC membrane demonstrated the formation of rosette arrangements. As a result, the more severe gypsum scaling together with contrasted gypsum crystal morphology suggested different gypsum scaling mechanisms for CTA and TFC membrane. ATR-FTIR spectra and XPS scans proved that the gypsum scaling on CTA membrane was dominated by bulk crystallisation with subsequent deposition; while that on the TFC membrane was driven by surface crystallisation via specific interaction between carboxylic functional groups and calcium ions. Specifically, the largely unchanged ratio of wavenumbers 1740 cm^{-1} (C=O stretching) to 1366 cm^{-1} (C-O stretching) on the CTA membrane indicated no interaction between gypsum and CTA membrane surface, which was also confirmed by the C1s XPS scan. In contrast, a gradual increase in the ratio of absorbance at wavenumbers of 3400 cm^{-1} to 2970 cm^{-1} was observed as gypsum scaling progressed on the TFC membrane. This specific interaction between carboxylic functional groups with calcium ions was also revealed by C1s XPS scan where the occurrence of the

carboxylate functional group at binding energy of 288.1 eV was found on the TFC membrane after gypsum scaling.

5. Acknowledgements

M.X. thanked Victoria University for the award of a Vice Chancellor Early Career Fellowship. Dr. Yichao Wang (Royal Melbourne Institute of Technology) was thanked for the discussion and technical assistance in XPS analysis.

6. References

[1] B. Mi, M. Elimelech, Chemical and physical aspects of organic fouling of forward osmosis membranes, Journal of Membrane Science, 320 (2008) 292-302.

[2] B. Mi, M. Elimelech, Organic fouling of forward osmosis membranes: Fouling reversibility and cleaning without chemical reagents, Journal of Membrane Science, 348 (2010) 337-345.

[3] C. Boo, M. Elimelech, S. Hong, Fouling control in a forward osmosis process integrating seawater desalination and wastewater reclamation, Journal of Membrane Science, 444 (2013) 148-156.

[4] S. Lee, C. Boo, M. Elimelech, S. Hong, Comparison of fouling behavior in forward osmosis (FO) and reverse osmosis (RO), Journal of Membrane Science, 365 (2010) 34-39.

[5] J.R.B. Herron, Edward G. Salter, Robert, Direct osmotic concentration contaminated water, in, OSMOTEK, INC., 1997.

[6] R.W. Holloway, A.E. Childress, K.E. Dennett, T.Y. Cath, Forward osmosis for concentration of anaerobic digester centrate, Water Research, 41 (2007) 4005-4014.

[7] A. Achilli, T.Y. Cath, E.A. Marchand, A.E. Childress, The forward osmosis membrane bioreactor: A low fouling alternative to MBR processes, Desalination, 239 (2009) 10-21.

[8] E.R. Cornelissen, D. Harmsen, K.F. de Korte, C.J. Ruiken, J.-J. Qin, H. Oo, L.P. Wessels, Membrane fouling and process performance of forward osmosis membranes on activated sludge, Journal of Membrane Science, 319 (2008) 158-168.

[9] T.Y. Cath, S. Gormly, E.G. Beaudry, M.T. Flynn, V.D. Adams, A.E. Childress, Membrane contactor processes for wastewater reclamation in space: Part I. Direct osmotic concentration as pretreatment for reverse osmosis, Journal of Membrane Science, 257 (2005) 85-98.

[10] M. Xie, L.D. Nghiem, W.E. Price, M. Elimelech, Toward Resource Recovery from Wastewater: Extraction of Phosphorus from Digested Sludge Using a Hybrid Forward Osmosis–Membrane Distillation Process, Environmental Science & Technology Letters, 1 (2014) 191-195.

[11] M. Xie, L.D. Nghiem, W.E. Price, M. Elimelech, A Forward Osmosis–Membrane Distillation Hybrid Process for Direct Sewer Mining: System Performance and Limitations, Environmental Science & Technology, 47 (2013) 13486-13493.

[12] R. Wang, L. Shi, C.Y. Tang, S. Chou, C. Qiu, A.G. Fane, Characterization of novel forward osmosis hollow fiber membranes, Journal of Membrane Science, 355 (2010) 158-167.

[13] J. Wei, C. Qiu, C.Y. Tang, R. Wang, A.G. Fane, Synthesis and characterization of flat-sheet thin film composite forward osmosis membranes, Journal of Membrane Science, 372 (2011) 292-302.

[14] N.Y. Yip, A. Tiraferri, W.A. Phillip, J.D. Schiffman, M. Elimelech, High Performance Thin-Film Composite Forward Osmosis Membrane, Environmental Science & Technology, 44 (2010) 3812-3818.

[15] X. Jin, J. Shan, C. Wang, J. Wei, C.Y. Tang, Rejection of pharmaceuticals by forward osmosis membranes, Journal of Hazardous Materials, 227–228 (2012) 55-61.

[16] M. Xie, L.D. Nghiem, W.E. Price, M. Elimelech, Relating rejection of trace organic contaminants to membrane properties in forward osmosis: Measurements, modelling and implications, Water Research, 49 (2014) 265-274.

[17] J. Wu, A.E. Contreras, Q. Li, Studying the impact of RO membrane surface functional groups on alginate fouling in seawater desalination, Journal of Membrane Science, 458 (2014) 120-127.

[18] Y. Mo, A. Tiraferri, N.Y. Yip, A. Adout, X. Huang, M. Elimelech, Improved Antifouling Properties of Polyamide Nanofiltration Membranes by Reducing the Density of Surface Carboxyl Groups, Environmental Science & Technology, 46 (2012) 13253-13261.

[19] B. Mi, M. Elimelech, Gypsum Scaling and Cleaning in Forward Osmosis: Measurements and Mechanisms, Environmental Science & Technology, 44 (2010) 2022-2028.

[20] B. Mi, M. Elimelech, Silica scaling and scaling reversibility in forward osmosis, Desalination, 312 (2013) 75-81.

[21] T.Y. Cath, A.E. Childress, M. Elimelech, Forward osmosis: Principles, applications, and recent developments, Journal of Membrane Science, 281 (2006) 70-87.

[22] J.R. McCutcheon, M. Elimelech, Influence of membrane support layer hydrophobicity on water flux in osmotically driven membrane processes, Journal of Membrane Science, 318 (2008) 458-466.

[23] R.L. McGinnis, N.T. Hancock, M.S. Nowosielski-Slepowron, G.D. McGurgan, Pilot demonstration of the NH3/CO2 forward osmosis desalination process on high salinity brines, Desalination, 312 (2013) 67-74.

[24] T.Y. Cath, M. Elimelech, J.R. McCutcheon, R.L. McGinnis, A. Achilli, D. Anastasio, A.R. Brady, A.E. Childress, I.V. Farr, N.T. Hancock, J. Lampi, L.D. Nghiem, M. Xie, N.Y. Yip, Standard Methodology for Evaluating Membrane Performance in Osmotically Driven Membrane Processes, Desalination, 312 (2013) 31-38.

[25] M. Xie, J. Lee, L.D. Nghiem, M. Elimelech, Role of pressure in organic fouling in forward osmosis and reverse osmosis, Journal of Membrane Science, 493 (2015) 748-754.

[26] S. Temmel, W. Kern, T. Luxbacher, Zeta potential of photochemically modified polymer surfaces, in: Progress in Colloid and Polymer Science, 2006, pp. 54-61.

[27] V.T. Do, C.Y. Tang, M. Reinhard, J.O. Leckie, Degradation of Polyamide Nanofiltration and Reverse Osmosis Membranes by Hypochlorite, Environmental Science & Technology, 46 (2012) 852-859.

[28] V.T. Do, C.Y. Tang, M. Reinhard, J.O. Leckie, Effects of Chlorine Exposure Conditions on Physiochemical Properties and Performance of a Polyamide Membrane—Mechanisms and Implications, Environmental Science & Technology, 46 (2012) 13184-13192.

[29] C.Y. Tang, Y.-N. Kwon, J.O. Leckie, Probing the nano- and micro-scales of reverse osmosis membranes—A comprehensive characterization of physiochemical properties of uncoated and coated membranes by XPS, TEM, ATR-FTIR, and streaming potential measurements, Journal of Membrane Science, 287 (2007) 146-156.

[30] C.Y. Tang, Y.-N. Kwon, J.O. Leckie, Effect of membrane chemistry and coating layer on physiochemical properties of thin film composite polyamide RO and NF membranes: I. FTIR and XPS characterization of polyamide and coating layer chemistry, Desalination, 242 (2009) 149-167.

[31] C.Y. Tang, Y.-N. Kwon, J.O. Leckie, Effect of membrane chemistry and coating layer on physiochemical properties of thin film composite polyamide RO and NF membranes: II. Membrane physiochemical properties and their dependence on polyamide and coating layers, Desalination, 242 (2009) 168-182.

[32] A. Tiraferri, M. Elimelech, Direct quantification of negatively charged functional groups on membrane surfaces, Journal of Membrane Science, 389 (2012) 499-508.

[33] M. Elimelech, C.R. O'Melia, Effect of electrolyte type on the electrophoretic mobility of polystyrene latex colloids, Colloids and Surfaces, 44 (1990) 165-178.

[34] A.E. Childress, M. Elimelech, Effect of solution chemistry on the surface charge of polymeric reverse osmosis and nanofiltration membranes, Journal of Membrane Science, 119 (1996) 253-268.

[35] Y.-N. Kwon, J.O. Leckie, Hypochlorite degradation of crosslinked polyamide membranes: II. Changes in hydrogen bonding behavior and performance, Journal of Membrane Science, 282 (2006) 456-464.

[36] C. Qiu, L. Setiawan, R. Wang, C.Y. Tang, A.G. Fane, High performance flat sheet forward osmosis membrane with an NF-like selective layer on a woven fabric embedded substrate, Desalination, 287 (2012) 266-270.

[37] Y. Wang, F. Wicaksana, C.Y. Tang, A.G. Fane, Direct Microscopic Observation of Forward Osmosis Membrane Fouling, Environmental Science & Technology, 44 (2010) 7102-7109.

[38] M. Xie, L.D. Nghiem, W.E. Price, M. Elimelech, Impact of organic and colloidal fouling on trace organic contaminant rejection by forward osmosis: Role of initial permeate flux, Desalination, 336 (2014) 146-152.

[39] S. Zou, Y.-N. Wang, F. Wicaksana, T. Aung, P.C.Y. Wong, A.G. Fane, C.Y. Tang, Direct microscopic observation of forward osmosis membrane fouling by microalgae: Critical flux and the role of operational conditions, Journal of Membrane Science, 436 (2013) 174-185.

513 [40] T. Kondo, The assignment of IR absorption bands due to free hydroxyl groups in cellulose,
514 Cellulose, 4 (1997) 281-292.

515 [41] H. Ju, X. Feng, Y. Ye, L. Zhang, H. Pan, C.T. Campbell, J. Zhu, Ca Carboxylate Formation
516 at the Calcium/Poly(methyl methacrylate) Interface, The Journal of Physical Chemistry C, 116
517 (2012) 20465-20471.

518 [42] M. Karra-Châabouni, I. Bouaziz, S. Boufi, A.M. Botelho do Rego, Y. Gargouri, Physical
519 immobilization of Rhizopus oryzae lipase onto cellulose substrate: Activity and stability studies,
520 Colloids and Surfaces B: Biointerfaces, 66 (2008) 168-177.

521

522

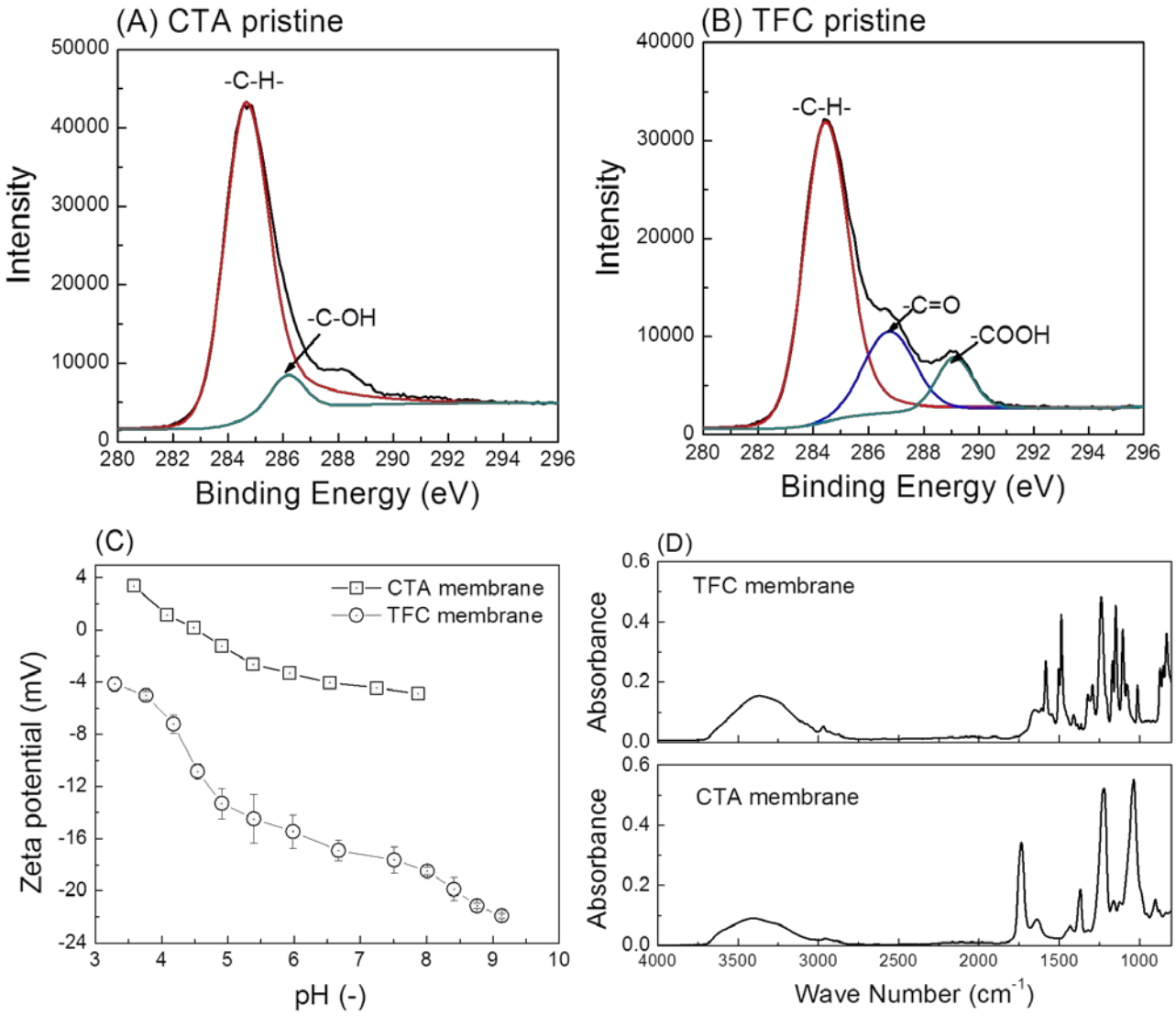

Figure 1: Key membrane surface chemistry properties of asymmetric cellulose triacetate (CTA) and thin-film composite (TFC) polyamide membranes. C1s binding energy of (A) CTA and (B) TFC membranes by X-ray photoelectron spectroscopy, showing the major functional groups on membrane surface; (C) Zeta potential of the CTA and TFC membranes as a function of solution pH, demonstrating membrane surface charge. Error bars represent a standard deviation from four replicate measurements using two membrane samples; (D) Representative attenuated total reflectance-Fourier transform infrared (ATR-FTIR) absorbance spectra for the CTA and TFC membranes.

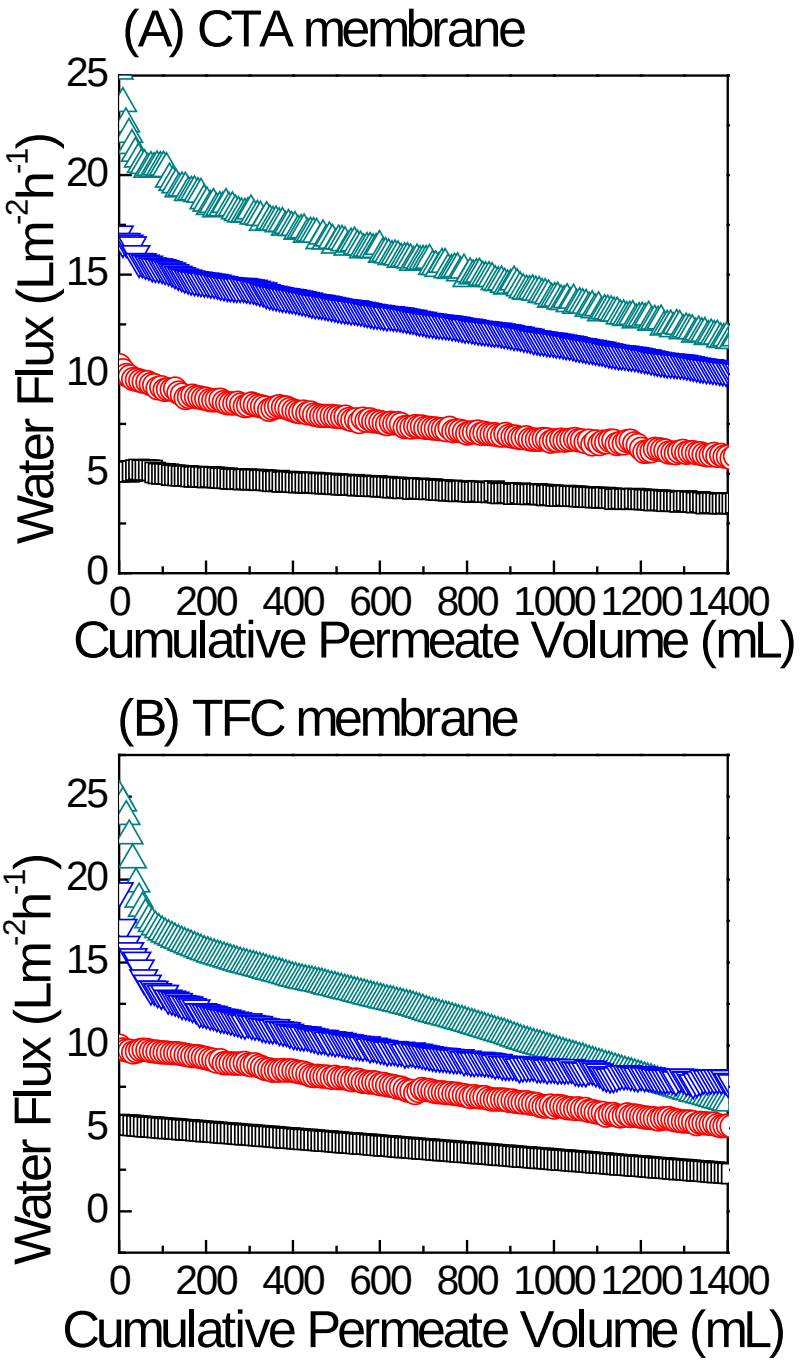

533
534
535 **Figure 2**: Water flux of gypsum scaling by (A) CTA and (B) TFC membrane. Experimental
536 conditions: feed solution was comprised of 35 mM $CaCl_2$, 20mM Na_2SO_4, and 19 mM NaCl. For
537 the CTA membrane, concentrations of draw solution to induce initial water fluxes of 5, 10, 15,
538 and 25 $Lm^{-2}h^{-1}$ were 0.35, 0.6, 1.5, and 2.5 M NaCl, respectively; for the TFC membrane, those
539 were 0.1, 0.4, 1, and 2 M NaCl, respectively. Cross-flow rate was 1 L/min (corresponding to the
540 cross-flow velocity of 8.5 cm/s). Temperatures of feed and draw solutions were 25.0 ± 0.1 °C.
541 Scaling experiment was operated for around 25 hours, attaining cumulative permeate volume of
542 1.4 L.

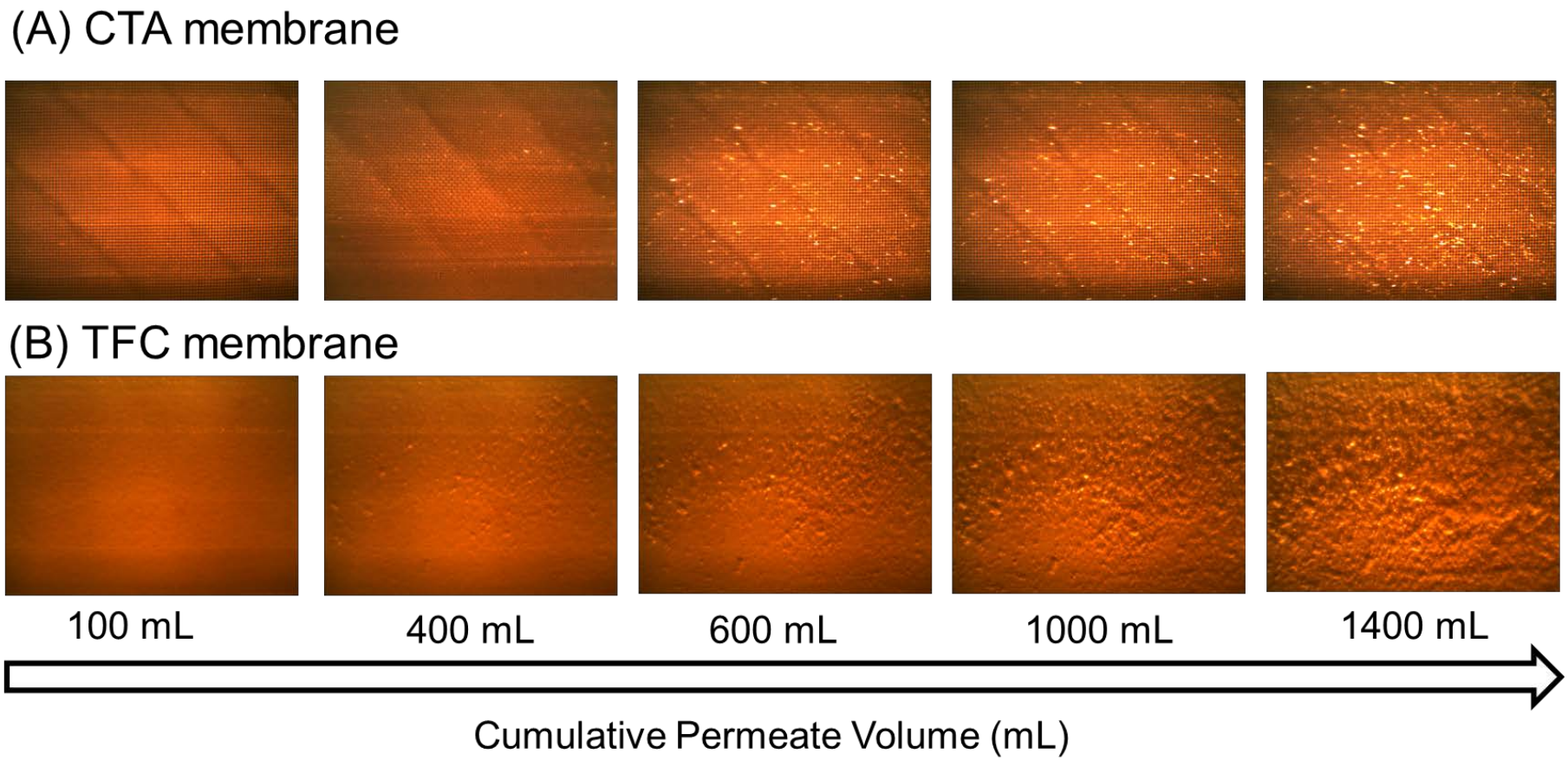

Figure 3: Representative images of gypsum scaling as a function of cumulative permeate volume for (A) CTA membrane and (B) TFC membrane. The images were captured by a real-time observation forward osmosis filtration system, and were used to calculate the membrane surface coverage in Figures 4 and 5. Experimental conditions were described in Figure 1.

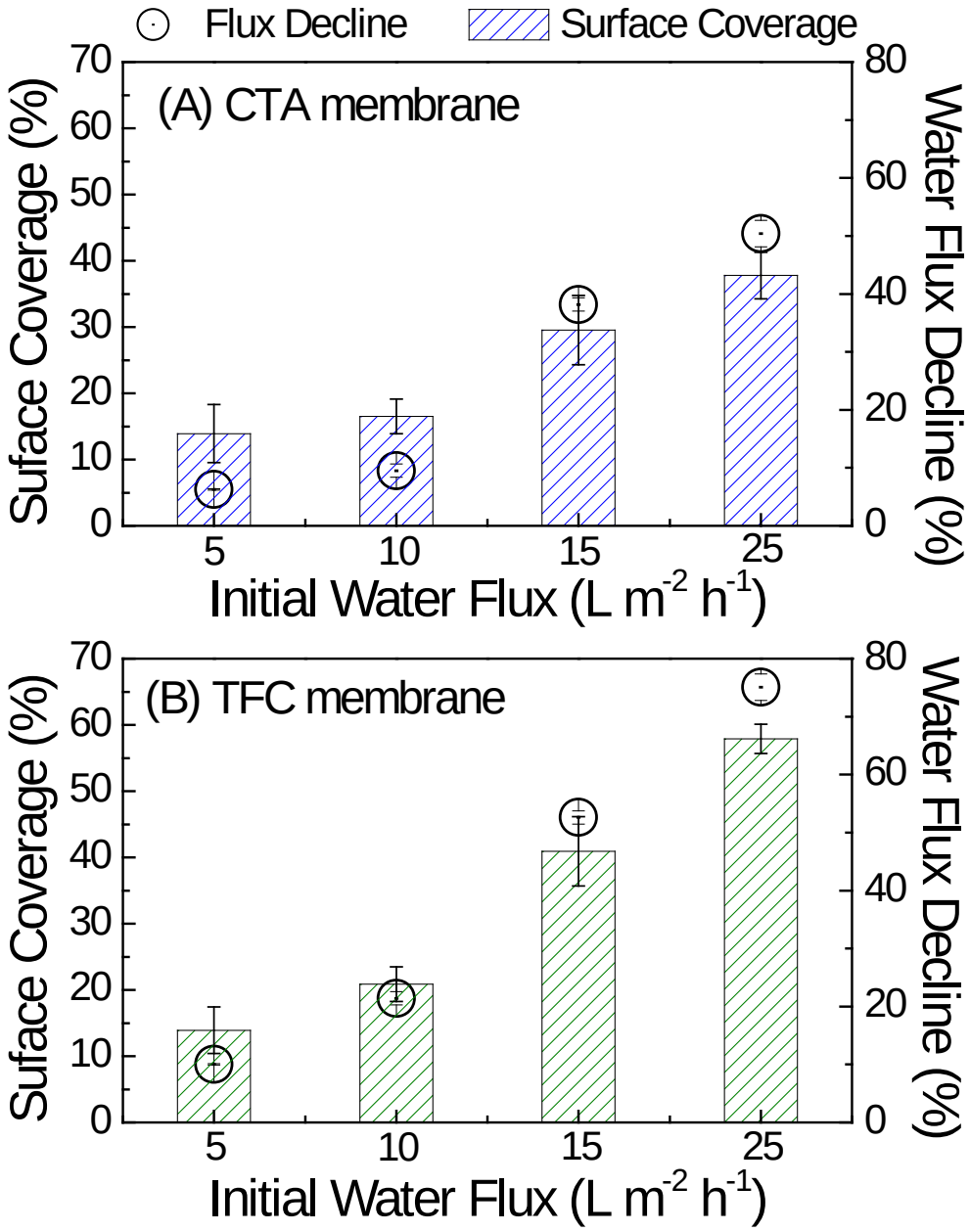

548
549
550 **Figure 4:** Water flux decline and membrane surface coverage as a function of initial water fluxes
551 for (A) CTA membrane and (B) TFC membrane. Membrane surface coverage was calculated
552 from images captured from real-time observation system with Image J and Photoshop.
553 Experimental conditions were as described in Figure 1.

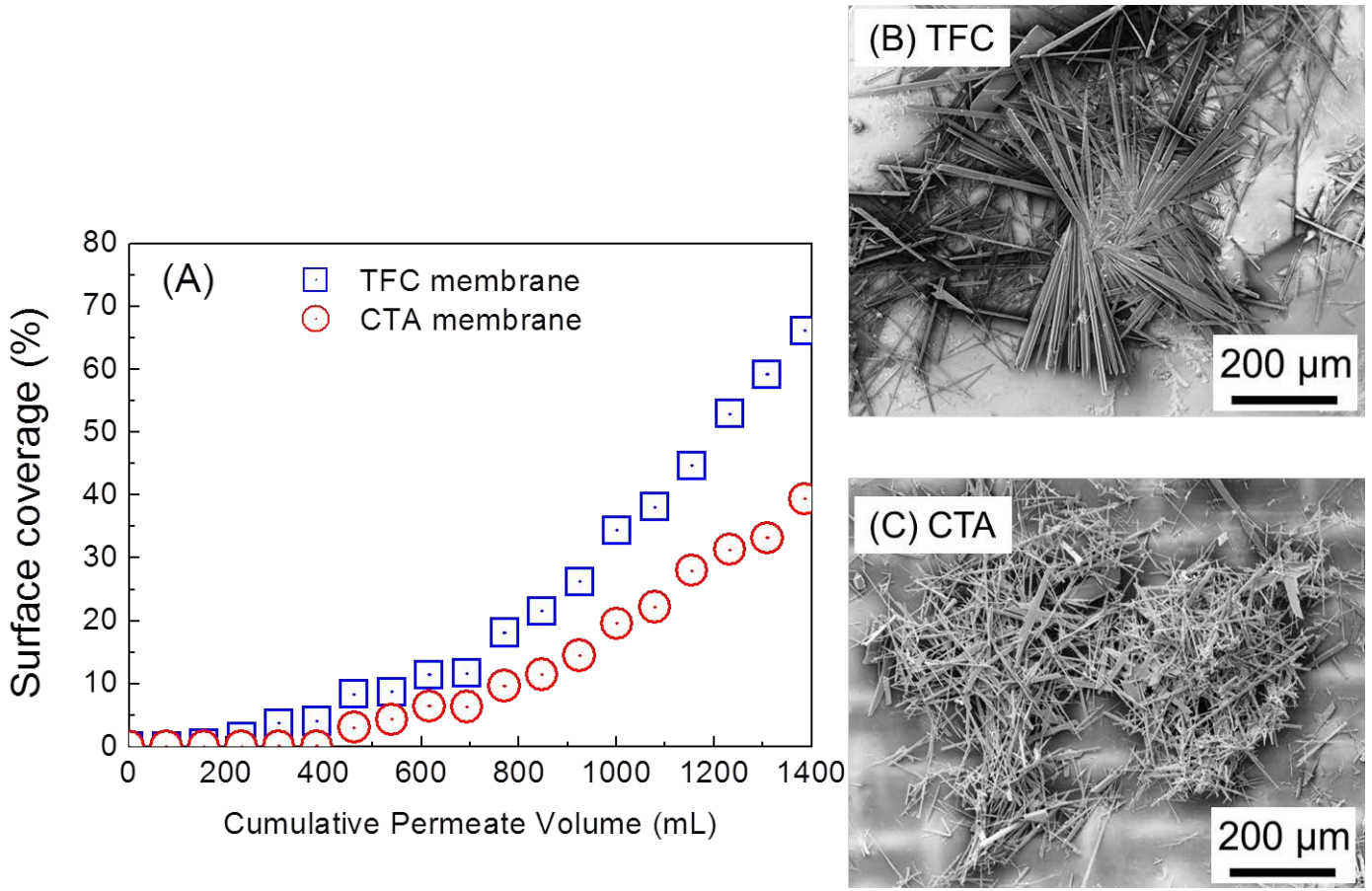

Figure 5: (A) Comparison of membrane surface coverage between CTA and TFC membranes as a function of cumulative permeate volume. Representative gypsum crystal morphology at the conclusion of scaling experiment on (B) TFC membrane and (C) CTA membrane. Experimental conditions were: feed solution contained 35 mM $CaCl_2$, 20mM Na_2SO_4, and 19 mM NaCl. Draw solution concentrations was 2 and 2.5 M NaCl for TFC and CTA membrane, respectively. Cross-flow rate was 1 L/min (corresponding to the cross-flow velocity of 9 cm/s). Temperatures of feed and draw solutions were 20.0 ± 0.1 °C. Scaling experiment was operated for around 25 hours, attaining cumulative permeate volume of 1.4 L.

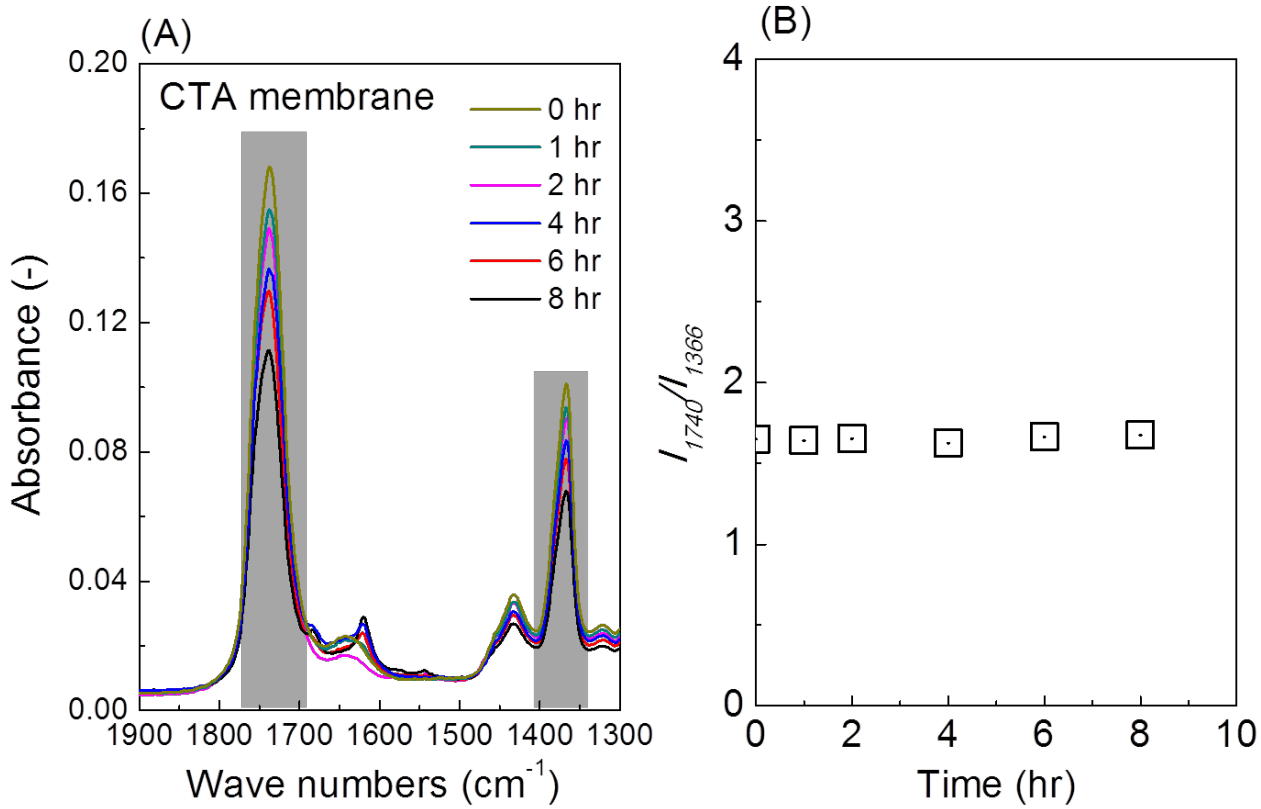
(A)
CTA membrane
0 hr
1 hr
2 hr
4 hr
6 hr
8 hr
Absorbance (-)
Wave numbers (cm-1)
(B)
I1740/I1366
Time (hr)

562

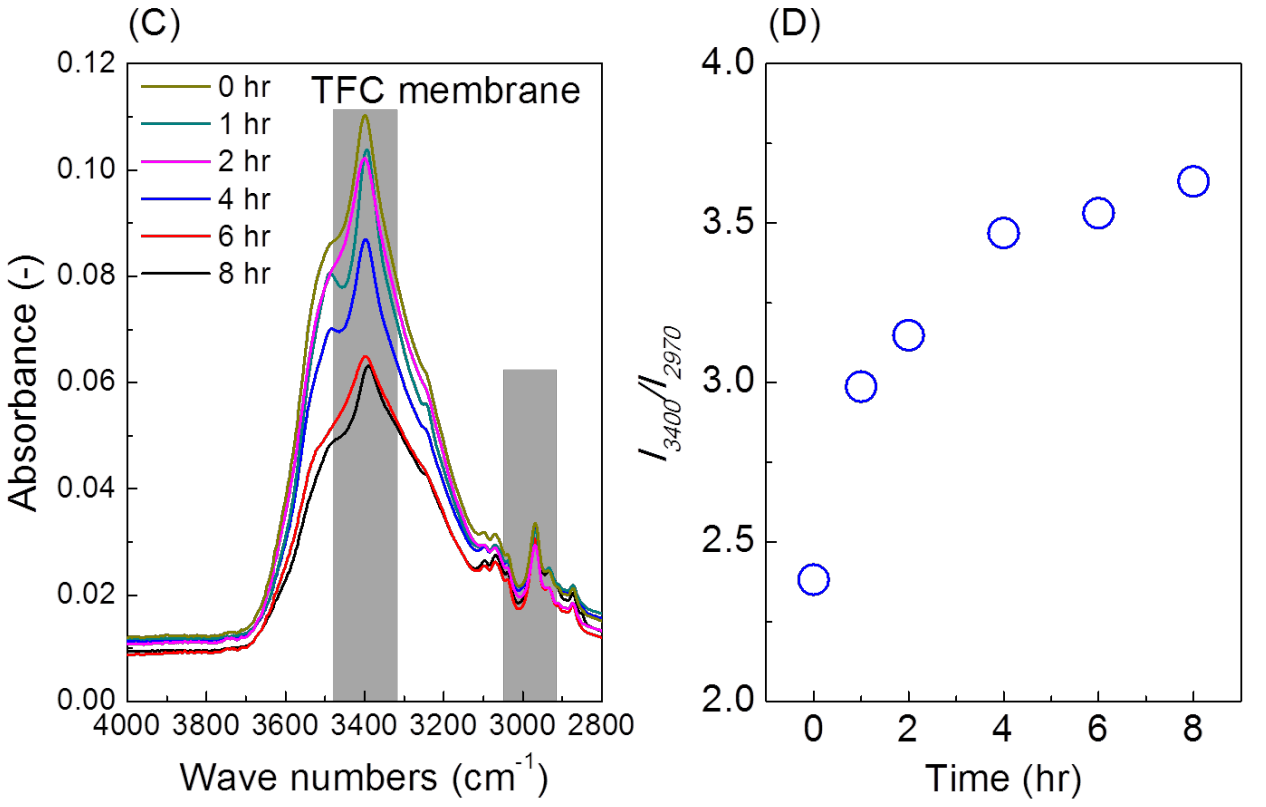
(C)
TFC membrane
0 hr
1 hr
2 hr
4 hr
6 hr
8 hr
Absorbance (-)
Wave numbers (cm-1)
(D)
I3400/I2970
Time (hr)

563

Figure 6: Representative attenuated total reflectance-Fourier transform infrared (ATR-FTIR) absorbance spectra for (A) CTA membrane and (C) TFC membrane at specific time intervals. The interaction between membrane surface and gypsum scaling was quantified as (B) ratio of absorbance at 1366 cm^{-1} (C-O stretching) to absorbance at 1740 cm^{-1} (C=O stretching) as a function of time for CTA membrane; and (D) ratio of absorbance at 2970 cm^{-1} (C-H stretching) to absorbance at 3400 cm^{-1} (O-H stretching) as a function of time for TFC membrane.

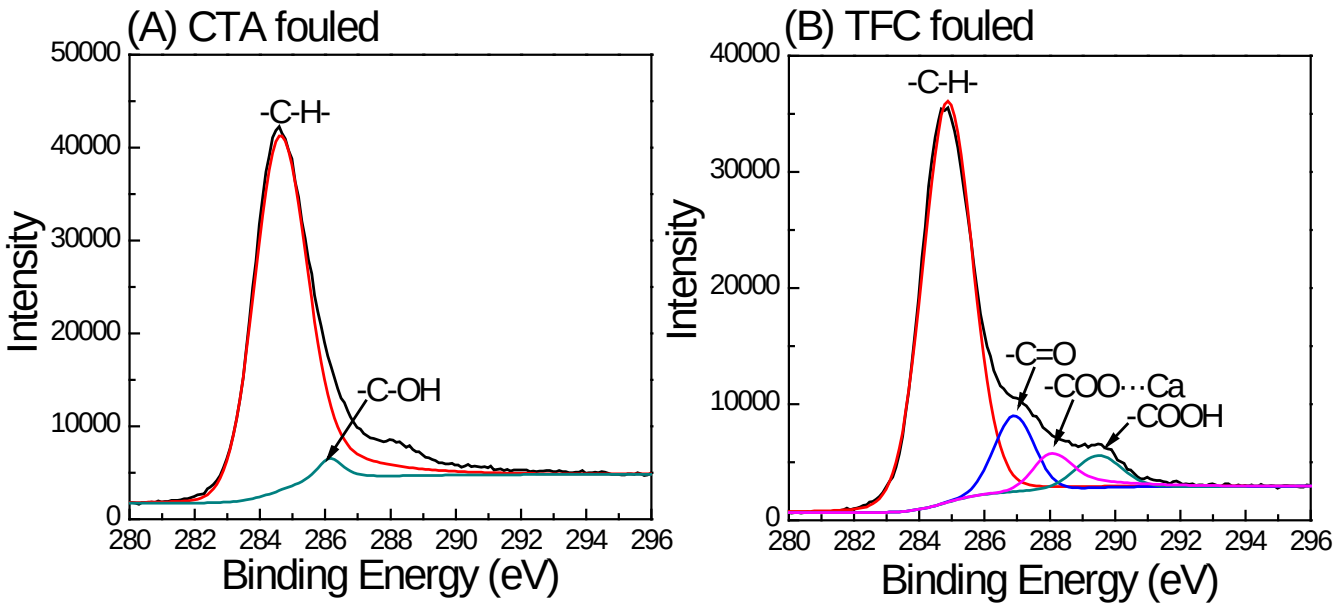

Figure 7: High resolution C1s scan by X-ray photoelectron spectroscopy of (A) CTA membrane and (B) TFC membrane at the conclusion of gypsum scaling. Binding energy of C1s was calibrated at 284.6 eV.